10-2019

A Simple Method to Characterize High Rate Twin Boundary Kinetics in Ni-Mn-Ga

Bibek Karki
Boise State University

Peter Müllner
Boise State University

Review of Scientific Instruments ARTICLE scitation.org/journal/rsi

A simple method to characterize high rate twin boundary kinetics in Ni-Mn-Ga

Cite as: Rev. Sci. Instrum. 90, 105107 (2019); doi: 10.1063/1.5109934
Submitted: 14 May 2019 • Accepted: 25 September 2019 •
Published Online: 14 October 2019

Bibek Karki,[1] Yotam Behar,[2] Itai Harel,[2] Eitan Caplan,[2] Arik Sabbag,[2] Doron Shilo,[2] Peter Mullner,[1] and Eilon Faran[2,a)]

AFFILIATIONS

[1] Boise State University, Boise, Idaho 83725, USA
[2] Technion – Israel Institute of Technology, Haifa 3200003, Israel

[a)] eilonfa@technion.ac.il

ABSTRACT

Experimental characterization of twin boundary kinetics is essential to systematically test and reproduce the actuation properties of Magnetic Shape Memory (MSM) elements at high rates. Here, we present a simple, nondestructive, experimental method to quantify the dynamic response of an MSM crystal and extract the major material properties that govern its kinetics. The tested sample is subjected to a mechanical pulse that is produced by a simple off-the-shelf solenoid. The mechanical pulse leads to actuation of the tested MSM Ni–Mn–Ga single crystal within 10 ms, during which the twin boundary velocity varies between zero and 2 m/s. The displacement and force in the MSM crystal are measured simultaneously using an optical sensor and a miniature force sensor, respectively. The data captured during a single loading experiment allow plotting a dynamic stress-strain curve as well as a kinetic relation that characterizes the macroscopic response of the crystal. In particular, the obtained kinetic relation enables the extraction of the transition driving force between slow (thermally activated) and fast (athermal) twin boundary motions. This transition driving force is a key material property that governs fast actuation capabilities of MSM elements. The macroscopic behavior of the sample is correlated with the motion of individual twin boundaries within the crystal by adding high speed microscopy to the experimental setup. This allows simultaneous high-rate tracking of individual twinning interfaces in Ni–Mn–Ga.

I. INTRODUCTION

Magnetic shape memory (MSM) alloys are candidate materials for fast actuation due to their ability to exhibit large and reversible displacements in the martensite phase.[1–5] The mechanical response of MSM can be driven either by a mechanical load or by a magnetic field, both of which promote the twinning reorientation process within the material. Twinning reorientation proceeds through the motion of individual twin boundaries, which are interfaces separating different martensite variants. Thus, the kinetics of individual twin boundaries under an external driving force (either mechanical, magnetic, or both) directly determines the macroscopic response of a given MSM crystal.[6,7] Because a major advantage of MSM over ordinary shape memory alloys is its ability to display a high frequency response under a cyclic magnetic field (typically in the 10–1000 Hz range), it is necessary to characterize the twin boundary motion at velocities and time scales that are relevant for MSM applications.

The most common experimental method used for evaluating the motion of twin boundaries in MSM is the uniaxial loading method, in which the crystal is deformed (usually in compression) at a constant strain rate while the force is recorded. Such experiments are performed at slow strain rates, typically smaller than 0.01 s^{-1}, and provide a quasistatic stress-strain curve (see, for example, Refs. 8–11). The resulting curve usually displays a long plateau of approximately constant stress, during which the twinning reorientation occurs. The average stress during the plateau is known as the twinning stress, which is a fundamental material property that represents the minimal stress required for the twin boundary motion. For example, uniaxial loading tests revealed substantial differences between the typical values of the twinning stress of type I (0.7–1 MPa) and type II (0.05–0.2 MPa) twins in MSM Ni–MN–Ga single crystals.[12–16]

While the twinning stress is an important property, it provides information only on the response of an MSM crystal at slow loading rates, which correspond to a complete twinning reorientation during

times longer than 10 s. In addition, kinetic measurements performed under a slow varying magnetic field (see, for example, Refs. 17 and 18) provide information that is relevant at velocities that are several orders of magnitude slower than typical actuation rates. Thus, complementary experimental methods must be employed to understand and quantify the kinetics of twinning over a wide range of velocities and, in particular, at velocities and time scales that match typical actuation rates, i.e., at the millisecond scale. In their recent works, Faran and Shilo measured the kinetics of individual twin boundaries in MSM Ni–Mn–Ga using pulsed magnetic field experiments.[19,20] This method involves the exposure of an MSM crystal to short (typically microsecond scale) magnetic pulses with a nearly constant amplitude throughout the majority of the pulse duration. The position of an individual twin boundary is tracked optically before and after each pulse, which allows calculating an average velocity value during each pulse. By performing a large number of pulsed experiments at different intensities of the magnetic field, twin boundary velocities were measured in Ni–Mn–Ga over nearly three decades (in the range of 0.01–10 m/s).[16] The kinetic relation for twin boundary motion was obtained by plotting the discrete velocity values as a function of the driving force.

The results obtained for Ni–Mn–Ga showed that the velocity of an individual twin boundary exhibits a sharp transition from slow (typically below 0.2 m/s) to much faster velocities at a distinct value of the driving force. A physical model was developed to explain this behavior,[19,20] and it predicted that the slow velocity regime corresponds to thermally activated motion (where the velocity follows an exponential dependence on the driving force), while the faster regime describes a-thermal motion, which follows a square root kinetic relation of the type

$$v_{TB} = \mu\sqrt{g^2 - g_o^2}. \quad (1)$$

Here, μ is the mobility coefficient, g is the driving force, and g_0 represents the transition value from one mechanism of motion to the other, which is associated with the energy required to overcome the lattice barrier for twin boundary motion (analogous to the Peierls barrier for dislocation motion).

The value of the transition driving force g_0 is 2–10 times larger than the value that corresponds to the twinning stress[6] and is of great engineering importance as it determines the magnetomechanical response of the MSM at time scales that are relevant for practical applications. Faran and Shilo showed that the performance of MSM actuators that are operated at frequencies above 1 Hz is determined mainly by g_0, while the twinning stress plays a minor role.[6,7] In addition, it was shown that the experimentally validated kinetic relations can be implemented in simple models that accurately predict and capture the dynamic response of an actual MSM Ni–Mn–Ga actuator.[21]

The above discussion emphasizes the importance in experimentally measuring the transition driving force g_0. This information is essential during the development of improved MSM crystals, as well as for quality control and regular production of existing compositions. Despite the satisfactory results obtained using the pulsed magnetic field method, it is relatively time-consuming and requires a large number of individual pulsed experiments to obtain the full kinetic behavior of a given crystal. In addition, a given set of pulsed magnetic field experiments typically provides kinetic information that characterizes only a small fraction of the tested crystal's volume. For example, under a 100 μs long magnetic pulse, at a velocity of 1 m/s, the twin boundary propagates about 0.1 mm. For a crystal whose length is 5 mm, the volume covered by the moving twin boundary during this pulse is only about 2% of the total volume of the crystal, thus providing only local information on twinning kinetics. Moreover, applying a well-controlled magnetic pulse at the microsecond time scale requires a complex experimental magnetic assembly, which is suitable mainly for small sized samples, typically not larger than 5 mm in length [see also similar pulsed magnetic field experiments reported by Ullakko *et al.* (Refs. 22 and 23)].

In principle, uniaxial loading experiments can be used for measuring twin boundary dynamics at high rates and for identifying g_0. Recently, Zreihan *et al.* performed sets of such experiments at different rates and showed that, for type II twins in monoclinic Ni–Mn–Ga, the plateau stress at the stress-strain curves increases at high rates.[24] In their fastest experiment, an almost complete twinning reorientation was obtained during 0.5 s, by going to the strain rate limit of a conventional material testing machine. Yet, the highest twin boundary velocity they obtained was 10^{-2} m/s, while the transition to the fast regime of the twin boundary motion occurs at velocities of approximately 0.2 m/s. Thus, these experiments could not reveal the value of g_0.

In this paper, we present an experimental approach that is simple, relatively inexpensive, and easy to operate, which allows extraction of the full twin boundary kinetics in a given MSM crystal from a single experiment. The tested MSM crystal is subjected to a uniaxial mechanical pulse at the millisecond time scale, while the displacement and force are measured simultaneously. Loading conditions are designed such that the strain rate during the mechanical pulse varies from zero (at the rest position) up to about 20 s^{-1}. Under these conditions, the twin boundary velocity varies within the interesting kinetic regime and the important kinetic parameters can be extracted. By comparing the obtained measurements with high-speed optical images that allow tracking the motion of individual twin boundaries, we conclude that the simple setup is adequate for obtaining the kinetics of an MSM single crystal. In particular, we show that this method allows the identification and extraction of the transition driving force from slow to fast twin boundary motion.

II. EXPERIMENTAL SETUP AND TEST PROCEDURE

The custom made mechanical setup is shown in Fig. 1. A commercial push-pull solenoid (GEEPLUS 301F) is used for applying uniaxial compression of the sample. This actuator is able to produce a mechanical load larger than 30 N over a stroke of 2 mm, within less than 15 ms. These capabilities are suitable for the stress and strain requirements (up to 10 MPa and 10%, respectively) of typical samples with a cross section area below 3 mm^2 and length below 20 mm.

The tested sample is placed within a designated groove in the base frame, between the solenoid's push rod and rigid support. In order to avoid proximity of the magnetic flux lines in the ferromagnetic push rod to the tested ferromagnetic sample (which may induce an additional, undesired, magnetic driving force for the twin boundary motion), a 6 mm long aluminum rod with a diameter of

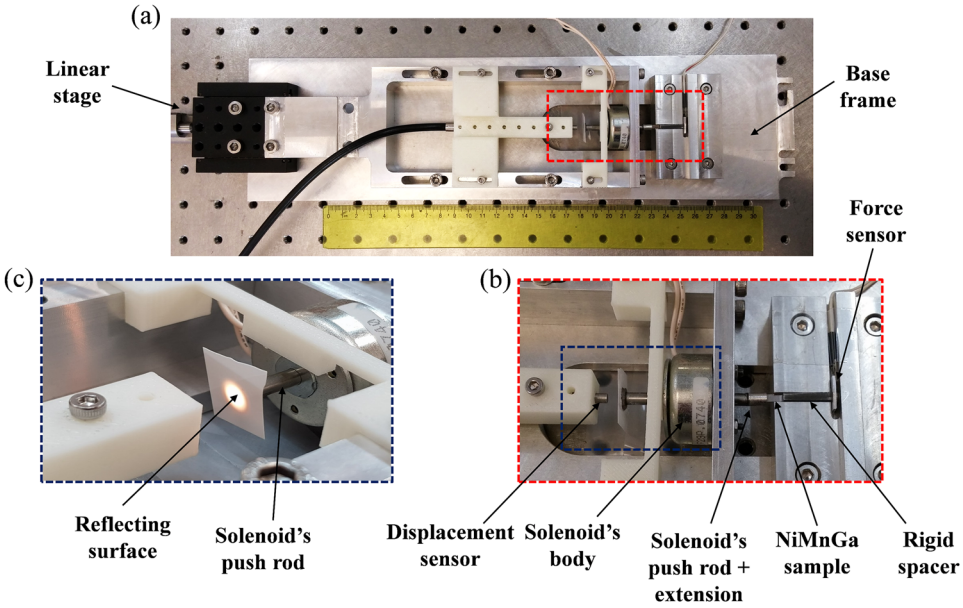

FIG. 1. (a) Overall image of the base frame and setup for the experiments. The 30 cm ruler serves as a scale bar for the setup. (b) Zoom in on the region of interest that shows the setup of the sample, force sensor, and optical displacement sensor. The solenoid's push rod provides mechanical load, and the attached extension eliminates its magnetic effect on the MSM element. The rigid spacer is required because of the MSM sample dimension. (c) Further zoom in on the solenoid region for a detailed optical displacement sensor setup. The reflecting surface is attached to improve the optical signal.

4 mm was firmly attached (glued) to the front end of the push rod, i.e., to the end that forms contact with the sample [Fig. 1(b)].

A miniature force sensor, FlexiForce, type A-201, with a thickness of 0.2 mm is placed between the sample and the base frame and measures the compression force developed in the sample. The force sensor has a typical response time of 5 μs. The system is designed to accommodate samples of up to 20 mm in length. For shorter samples, such as the 5 mm long crystal reported in this work, an additional rigid steel spacer was inserted between the sample and the force sensor [Fig. 1(b)].

The position of the solenoid's push rod is measured continuously using an optical sensor, MTI 2100 Fotonic sensor, which tracks the back end of the push rod. The optical sensor has a resolution of about 1 μm and a frequency response of 150 kHz. A thin alumina sheet was glued to the push rod's back end to improve the reflectance of the optical signal [Fig. 1(c)]. Since the plunger is in direct contact with the sample's end, displacement measurement of the push rod provides approximate change in the length of the tested sample, which allows calculating its macroscopic strain (the total displacement error introduced by elastic deformations of the push rod, the extension aluminum rod, and the steel spacer is less than 0.3 μm).

Overall, the mass of the plunger including the added parts described above is 17 g. Acceleration of this finite mass has some inertial effect, particularly during the first stages of the loading pulse. However, the force sensor measures the resultant force applied directly on the tested sample, and thus, this effect is already taken into account and does not require a separate evaluation.

We measured the kinetics in a 10M $Ni_{50.0}Mn_{28.3}Ga_{21.7}$ (at. %) single crystal obtained from AdaptaMat, Ltd. The sample size was 2.5 × 0.9 × 5.3 mm^3 when fully elongated, and the sample faces were cut along {100} planes of the parent austenite phase. Loading tests were performed along the long, 5.3 mm, axis of the crystal. All measurements were performed at room temperature, at which the crystal is fully in the martensite phase. The transformation temperature from martensite to austenite for this composition is about 50 °C. The crystallographic structure of the martensite is monoclinic, which gives rise to the appearance of both type I and type II twinning modes. For both types of twins, the magnitude of the axial twinning strain is about 6% (Refs. 12 and 25). Thus, for a 5.3 mm long sample, a total displacement of about 0.32 mm is expected when the sample is completely switched from one twin variant to another.

Prior to each test, the sample was elongated along its 5 mm axis and brought to a state of a single martensite variant. This was achieved by placing it inside a dedicated magnet assembly. The crystal was then inserted into the loading system, and the plunger position was adjusted using a precision linear stage to obtain a small preload of about 0.2 N. This preload ensured that all gaps between the plunger, sample, force sensor, and the rigid support are eliminated prior to the activation of the solenoid.

The proposed setup is positioned under an optical microscope (Olympus BX51) equipped with Nomarski interference contrast imaging and a high-speed camera (Photron's FASTCAM Mini AX200 camera). Fast imaging was performed at a rate of 20 000 frames/s, with an image size of 704 × 384 pixels and an exposure time of 1.05 μs for each frame. An objective magnification of 5 resulted in a field of view of approximately 5.5 × 3.0 mm^2, which allowed capturing the entire surface area of the sample. Under these conditions, each pixel in the captured image corresponds to 7.9 μm on the sample. We emphasize that the use of an optical microscope and a high-speed camera is not an essential part of the proposed method and is employed only to evaluate and validate its performance.

Trained Ni–Mn–Ga single crystals typically contain few twin boundaries that span the entire cross section of the sample. These are characteristics to crystals produced by the former Adaptamat (which

is tested in this work) as well as to crystals produced to date by other manufacturers, such as ETO magnetics (see, for example, Refs. 26, 10, 27, and 28). Thus, under most conditions, the number and location of twin boundaries observed at the top surface provide a reliable indication of the bulk structure (e.g., when the distance between adjacent twin boundaries as well as the distance between a twin boundary and the sample edges is larger than the sample's thickness). In addition, previous studies have shown that twin boundary motion is symmetric with respect to tension or compression, during quasistatic loading as well as under high rate loading (see, for example, Refs. 10, 20, and 29). This can be reasoned by the fact that in crystals that contain few twin boundaries, the distance between adjacent twins is large and thus the interaction between twin boundaries is negligible.

III. IMAGE ANALYSIS

The high-speed camera provided grayscale images with the 8-bit dynamic range. This implies that each pixel in the images is assigned with a value between 0 and 255, representative of its grayscale brightness (see the scale bar in Fig. 2). The displacement of the twin boundary along the crystal's long axis was obtained by systematically evaluating pairs of consecutive images [e.g., Figs. 2(a) and 2(b)]. First, we calculated the absolute difference between two images, i.e., the brightness difference of each pixel in the two images, as seen in Fig. 2(c). An auxiliary parameter α was defined to provide a threshold on the image contrast after obtaining the absolute difference; if the brightness difference for a given pixel is larger than α, the twin boundary displacement is accepted and the pixel is assigned as white; otherwise, it is disregarded and the pixel is assigned as black. The resulting white-black binary image of the absolute difference contrast is shown in Fig. 2(d). An optimal value of the threshold parameter was set to $\alpha = 50$.

In order to remove noise from the binary contrast image [Fig. 2(d)], an additional algorithm was applied on each column of the binary image. The algorithm groups consecutive indices of white pixels for each column and ignores those groups that consist of only one element in the column. If there is an isolated white pixel that does not share a neighbor up or down in the column, the pixel is considered as a noise and is assigned as black. The resulting filtered binary image is shown in Fig. 2(e). The twin boundary displacement for a given column is taken as the total number of the grouped white pixels after filtering the noise. The total displacement of the twin boundary for a given filtered binary image is taken as the average of the number of grouped white pixels across nonzero columns (i.e., columns in which grouped white pixels were identified). We note that some columns might accept noise as a valid twin boundary displacement, for example, an isolated pair of two consecutive white pixels. However, since the average displacement across the nonzero columns is considered, most of the noise is suppressed. The above algorithm implies that the minimal detection limit for the twin boundary displacement for each time step is two pixels. This limitation corresponds to detection capability of velocities larger than 0.22 m/s. For displacements larger than two pixels, a resolution better than one pixel is obtained due to the averaging over all columns. Based on the obtained data, we evaluate the velocity resolution to be 0.05 m/s.

A twin boundary in Ni–Mn–Ga lies approximately on {110} planes and is thus inclined at nearly 45° with respect to the {100} planes of the parent austenite phase, which, in our case, are the surface planes of the crystal. Thus, the magnitude of the displacement of the twin boundary observed on the surface is larger by a factor of

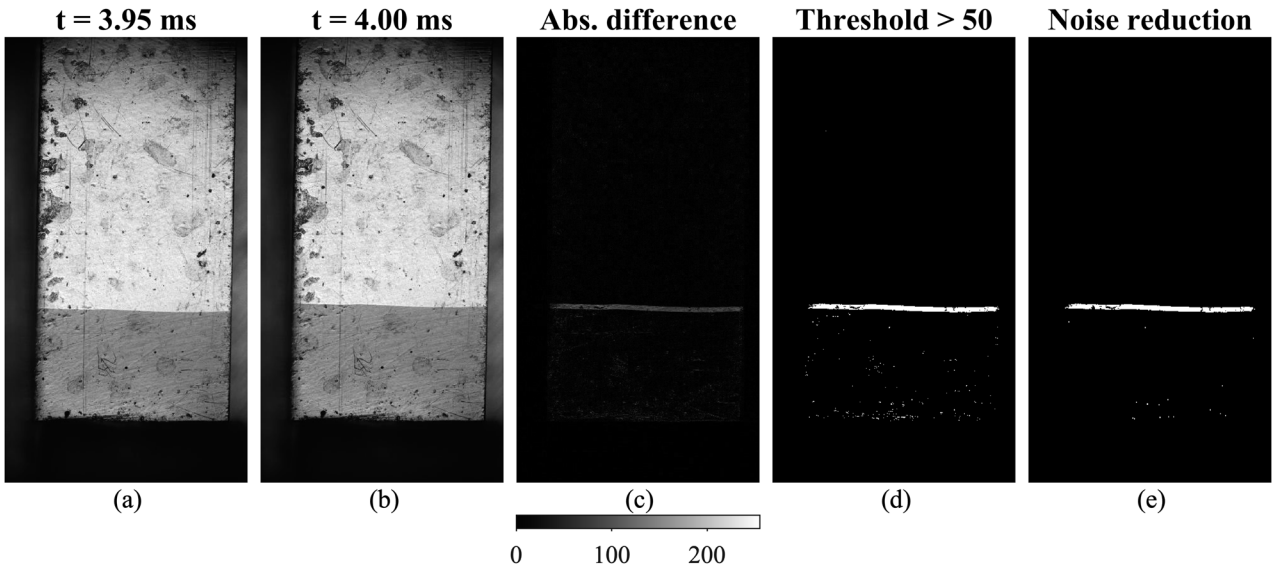

FIG. 2. Calculating twin boundary displacement from microscope images. [(a) and (b)] A typical pair of consecutive images, showing an individual twin boundary propagating along the sample. (c) The absolute grayscale difference between images (b) and (a). (d) A binary image map obtained from image (c) by setting a threshold value on the absolute difference. (e) Filtered binary image after noise reduction. The twin boundary displacement is calculated by averaging the number of white pixels in the filtered image (see the text for details). The intensity scale bar displays the 256 grayscale levels in images (a)–(c).

$\sqrt{2}$ relative to the normal displacement of the twin boundary (see Ref. 20). Thus, the "true" displacement of the twin boundary (i.e., perpendicular to the boundary plane) is taken as the value measured on the surface multiplied by a factor of $1/\sqrt{2}$.

IV. RESULTS

Typical profiles of the force, sample's displacement, and twin boundary displacement as a function of time are shown in Figs. 3(a)–3(c). The displacement of the sample reaches a maximal value of 0.33 mm after about 12 ms. This value is in accordance with the 6% twinning strain corresponding to $c/a = 0.94$ (c and a are the lattice parameters of the unit cell) and indicates that the entire crystal has completely twinned during 12 ms, which corresponds to an average actuation frequency of about 40 Hz. At the same time, the maximal value of the twin boundary displacement recorded by using the high speed camera is smaller than 2.5 mm and is equivalent to only 3% strain. This implies that additional twin boundaries that were not visible in the microscopy images contributed to the total strain. This point will be elaborated further in this section.

The time derivatives of the displacement data [shown in Figs. 3(b) and 3(c)] represent the velocities of the sample and of the twin boundary. These data are shown in Fig. 4(a) alongside the force signal. Due to the lower sampling rate of the twin boundary displacement relative to the sample's displacement, the resulting twin boundary velocity data are noisier than the sample's velocity data. The twin boundary velocity changes between zero and about 1 m/s, thus covering the entire range that is relevant for practical applications and allows quantifying the full twinning kinetics.

The data displayed in Figs. 3(a)–3(c) allowed calculating two independent dynamic stress-strain curves, which are presented in Fig. 4(b). The first curve [blue in Fig. 4(b)] is obtained from the measured displacement of the sample, d_{sample} [Fig. 3(b)], and the strain is calculated as

$$\varepsilon_{sample} = d_{sample}/L, \tag{2}$$

where $L = 5.3$ mm is the sample length. The second curve [green in Fig. 4(b)] is obtained from the measured twin boundary displacement, d_{TB} [Fig. 3(c)], and the strain is calculated according

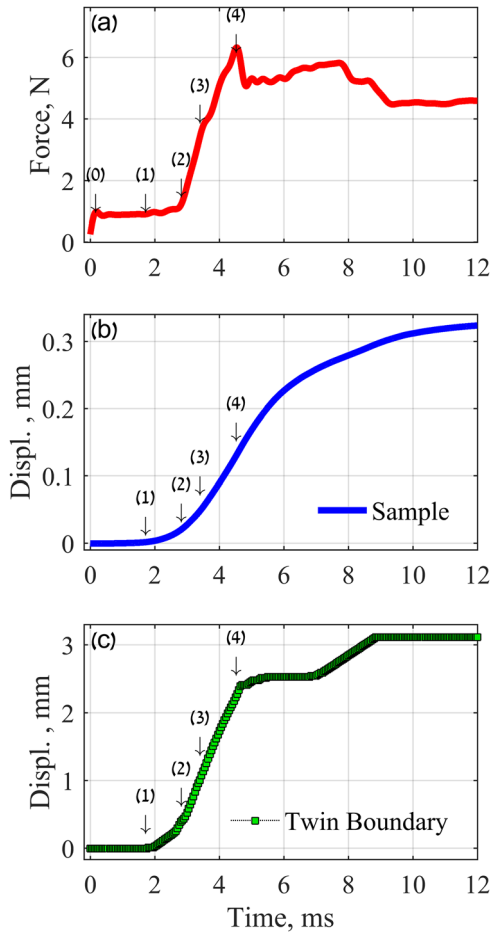

FIG. 3. Measured profiles of the force (a), sample displacement (b), and twin boundary displacement (c), taken from a pulsed loading test on the sample shown in Fig. 2. The numbered labels mark the same time points on all charts (see the text for details).

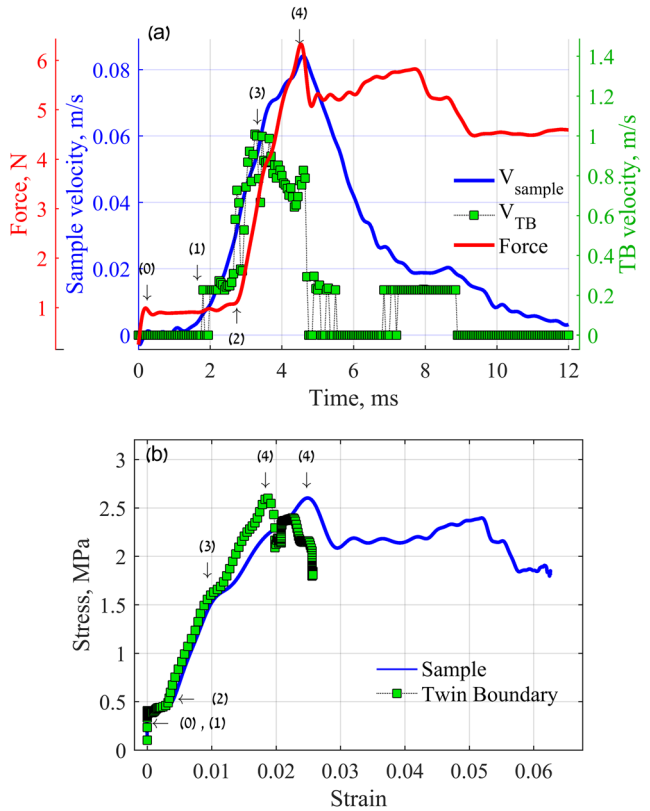

FIG. 4. (a) Calculated velocities of the sample (blue) and the twin boundary (green), overlaid on the measured force profile (red). (b) Stress-strain curves obtained from the two displacement-force measurements. The numbered labels mark the same time points shown in Fig. 3.

to

$$\varepsilon_{TB} = d_{TB} \times (1 - c/a)/L. \quad (3)$$

Here, we assume that only the single visible twin boundary [whose position is displayed in figure (c)] contributes to the total strain and thus multiplies its displacement by $(1 - c/a)$ (the longitudinal component of the twinning strain). The nearly perfect overlap between the two curves at strains smaller than 0.01 (equivalent to the first 4 ms of the experiment) indicates that this assumption is valid within this time period. For both stress-strain curves shown in (e), the stress is obtained by dividing the measured force by the initial cross section area of the Ni–Mn–Ga sample.

The shape of the stress-strain curve and the values of the stress shown in Fig. 4(b) are significantly different than common slow-rate stress-strain curves due to the high loading rate. In particular, in a typical slow-rate stress-strain curve, the initial sharp increase in stress is associated with a dominant elastic response with a negligible motion of twin boundaries.[6,24] In the dynamic stress-strain curve in Fig. 4(b), the initial increase of the stress describes a "pseudoelastic" response that involves a prominent twinning reorientation, as validated by the microscopy images.

Numbered markings that represent several important points in time are displayed on the different plots in Figs. 3 and 4. In the following, we discuss these points with respect to the characteristics of the experimental setup and the kinetics of twinning in the tested sample.

Point (0) marks a time of about 0.2 ms after the solenoid was activated. During this period, the force sensor shows a small increase in its reading from the preload value. This increase can be associated with the rise time of the magnetic field in the solenoid and the resulting magnetization of the push rod. No displacements were recorded during this short time, and thus, they do not appear in Figs. 3(b) and 3(c).

Around point (1), which corresponds to t = 1.6 ms, the displacement sensor and the optical images start detecting the motion of the sample and the twin boundary, respectively, while the force shows an initial increase above the value recorded at point (0). The higher spatial and temporal resolutions of the optical sensor relative to the camera images lead to a faster and continuous response of the sample's displacement relative to that of the twin boundary. In accordance, the velocities of the sample and the twin boundary display nonzero values around this point in time.

According to the specifications of the solenoid, its initial response time due to inertia associated with the mass of the push rod is 1–2 ms. This value is in accordance with the observed "dead-time" of about 1.6 ms. Since no motion is detected at times smaller than point (1), the stress-strain curves during this time also show zero strain.

While point (1) marks the beginning of motion, after an additional 1 ms, there is a sharp increase in the velocities of the sample and the twin boundary [marked as point (2)], which takes place during a relatively small increase in the force. The variations of the measured quantities suggest a change in the mechanism of the twin boundary motion. The value of the force around which the transition takes place is approximately 1 N, which corresponds to a stress of 0.45 MPa or a driving force of 30 kJ/m^3 (under mechanical loading, the driving force for the twin boundary motion is directly related to the uniaxial stress according to $g = \sigma\varepsilon$, where $\varepsilon = 1 - c/a$ is the twinning strain). The velocity of the twin boundary around this transition point is about 0.25 m/s. This value is in agreement with the one reported earlier for the transition from slower (thermally activated motion) to faster (a-thermal) motion.[6,20]

Approximately, 1 ms past point (2), i.e., at t = 3.7 ms, another transition is detected and is marked as (3). At this point, the velocity of the twin boundary starts decreasing, while that of the sample keeps increasing together with the force. This behavior can be reasoned by considering the start of the motion of additional twin boundaries in the sample, which are not visible in the optical images. For example, there may be an additional twin that nucleated at the bottom surface of the crystal, opposite to the surface that is observed by the microscope. Recalling that twin boundaries in Ni–Mn–Ga are inclined by 45° with respect to {100} planes, the additional twin can expand to a width of 1 mm (at the bottom surface) before penetrating to the top surface and be observed by the microscope.

On the stress-strain curves [Fig. 4(b)], point (3) marks the start of a deviation of the curve calculated based on the twin boundary displacement from the curve calculated from the sample displacement. As a result, the twin boundary curve exhibits smaller strains for similar stress values. This also supports our assumption that at this time additional twin boundary/boundaries start propagating in the sample and their motion also contributes to the overall macroscopic strain.

The last marked point (4) occurs at about t = 4.3 ms and marks a sudden and sharp decrease in the measured force from its peak value. This sudden drop in the force probably occurs because during this short time-segment, the velocity of the solenoid's push rod is slightly smaller than the contraction velocity of the sample. Yet, the force does not drop to zero, indicating that contact between the push rod and the sample is maintained during the entire time period. After additional few tenths of a millisecond, the force stabilizes, which implies that the velocities of the sample and the solenoid are equal again. The transient difference between the velocities of the push rod and the sample occurs probably due to the inertia of the push rod, which does not allow it to accelerate as fast as the sample's velocity changes.

V. DISCUSSION

The results presented in Sec. IV demonstrate the capabilities of the proposed experimental setup to measure and evaluate the mechanical response associated with the twin boundary motion in an MSM crystal subjected to a millisecond-scale load pulse. In the following, we use the measured data to evaluate and quantify the kinetics of the process. In particular, we extract the kinetic relations for the motion of twin boundaries for two different twin types. Kinetic relations are obtained independently from the measured sample displacement and the twin boundary displacement.

Figure 5 presents kinetic analysis for two different experiments on the same crystal. The visible twin boundaries in each case [Figs. 5(a) and 5(d)] have different macroscopic orientations with respect to the top surface plane of the sample (former {100} plane of the austenite phase). In Fig. 5(a), the projection of the twin boundary on the surface plane is generally parallel to the sample's directions,

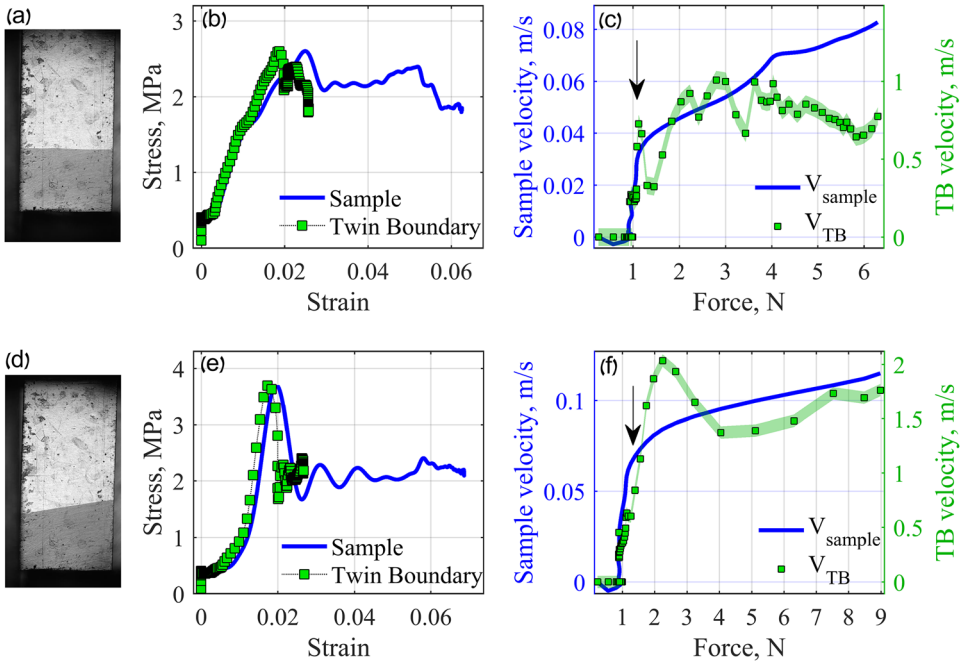

FIG. 5. Dynamic behavior of a Ni–Mn–Ga single crystal obtained from two different experiments conducted on the same sample. Experiment 1: (a)–(c). Experiment 2: (d)–(f). The visible twin boundary in each experiment is shown in (a) and (d). Stress-strain curves [(b) and (e)] are calculated independently for the sample and for the twin boundary from the entire measured data. Kinetic relations [(c) and (f)] are calculated independently for the sample and for the twin boundary, and include data recorded up to the stress peak in the stress-strain curves. The shaded area in light green represents the estimated measurement error in the twin boundary velocity.

while in Fig. 5(d), the projection is oriented at about 7° with respect to the surface plane.

The stress-strain curves obtained for the two experiments [Figs. 5(b) and 5(e)] show similar trends; an initial rise of the stress takes place at strain levels of up to about 0.02, followed by stabilization of the stress at a value of about 2.5 MPa during the remaining 0.04 strain range. The sharp stress drops at a strain of about 0.02 in both cases is a result of the experimental setup, as discussed in Sec. IV, and does not necessarily reflect on the intrinsic behavior of the tested material. We note that there are slow-rate loading tests that also display a stress drop due to nucleation and initiation of the twin boundary motion. In our experiments, twin boundary motion occurred already before the stress drop, and we did not observe nucleation of new twins during the force drop event.

The dynamics associated with the motion of twin boundaries are best characterized by the kinetic relation, which correlates the velocity of the process with the force that drives it, as presented in Figs. 5(c) and 5(f). Note that the kinetic relation figures are based only on data recorded up to the stress peak in Figs. 5(b) and 5(e), i.e., when the velocity of the push rod follows the contraction rate of the sample. Figures 5(c) and 5(f) present two types of kinetic relations. The first is a "macroscopic" kinetic relation that correlates between the contraction velocity of the sample and the applied force (blue line). The second is a "local" kinetic relation that was tracked using the optical images (green marks) and describes the dynamics of the visualized individual twin boundary. The error bars/regime in the velocity values of the twin boundary represent the measurement uncertainty that is dictated by the finite resolution of the optical camera, the filtering algorithm, and the frame rate, and is evaluated as ±0.05 m/s. We note that the scattering of the velocity data is larger than the measurement error (for similar values of the force) and thus indicates variations in the mobility of a twin boundary at different locations along the crystal. This phenomenon was also observed and reported in previous studies employing the pulsed magnetic field method.[16,19,20]

The vertical velocity axes of the kinetic relations in Figs. 5(c) and 5(f) are scaled by a factor of $1 - c/a$, which is the value of the twinning strain. In the case that a single twin boundary propagates along the sample, the two velocities must obey the kinematic relation $v_{TB} = v_{sample} \cdot (1 - c/a)$. Indeed, the "macroscopic" (sample) and "local" (twin boundary) kinetic relations obtained during each single experiment show very good agreement with the above relation during the first few milliseconds of the experiment, when only a single twin boundary propagated in the sample. Once the velocity of the imaged twin boundary decreases, the two relations deviate from each other: the sample's velocity keeps increasing with the force, while that of the imaged twin boundary decreases [see, for example, at forces larger than 4 N in Fig. 5(c)]. This behavior results when multiple twin boundaries start propagating in the sample, as discussed in Sec. IV.

The shape of the kinetic relation of the overall sample and that of the twin boundary show a transition from slow to fast motion, which takes place at a force of about 1 N as indicated by an arrow. This value is equivalent to a transition driving force of about $g_0 = 30$ kJ/m^3, which is comparable, but lower, than the values reported for the two twin types using the pulsed magnetic field method.[20,28,30] Moreover, the good correlation between the kinetic relation obtained from the twin boundary displacement and that obtained from the sample's displacement imply that the latter can serve as a good indication for the dynamic response of the tested crystal and, in particular, for the identification of the transition force g_0, which is an important material property. From an engineering perspective, the sample's kinetic relation provides a

macroscopic description of the sample's dynamic response. Thus, we conclude that the simple experimental setup presented in this work, even without the addition of an optical microscope and a high-speed camera, can serve as an efficient and convenient method for complete dynamic characterization of Ni–Mn–Ga crystals, particularly for determining the transition driving force g_0.

The differences between the stress train curves and between the kinetic relations obtained from the two experiments are minor [compare Fig. 5(b) with Fig. 5(e) and Fig. 5(c) with Fig. 5(f)]. This implies that the two twin boundaries shown in Figs. 5(a) and 5(d) have similar dynamic behavior. At the same time, the differences in the orientations of the two twins on the observed surface (which are also influenced by the accuracy at which the sample was cut relative to the {100} planes of the austenite phase) may suggest that the two boundaries are of different types. In order to rigorously identify the exact characteristics of a twin boundary and correlate them to the measured dynamic response, the following procedure can be followed: (1) create a twin boundary in the tested sample, (2) perform a detailed crystallographic analysis of the twin type with electron back scattered diffraction (EBSD) or x-ray diffraction (XRD) methods, and (3) perform a mechanical pulse test using the experimental system described in this work. We note that step (2) in the above procedure is beyond the scope of the current work, and thus was not pursued here.

Recent crystallographic studies of twin boundaries in Ni–Mn–Ga using EBSD and XRD have shown that mixed regions of type II and I can coexist along a single macro twin boundary (see Refs. 31–33), i.e., the same twin boundary can be of type I in certain regions of the sample and of type II in other regions. This complex microstructure is feasible through different arrangements of "micro" twins (typically referred to as modulation twins) across a "macro" twin boundary.[31,32] With such XRD and EBSD characterization methods, researchers can identify the type of twins, but are restricted to a small local region, typically not larger than few tens of micrometers. At the same time, optical microscopy images [similar to those in Figs. 5(a) and 5(d)] can capture an entire millimeter-scale macro twin boundary, but can only provide the average angle that the projection of the twin boundary forms on the observed surface (see also Refs. 12, 34, 20, and 32). However, when the macro twin boundary is composed of complex arrangements of modulation twins, this average angle is not always a precise indication of the type of the macro twin boundary, and at the millimeter-scale, most twin boundaries may be composed of a combination of the two types, as explained in Ref. 32. Our results (Fig. 5) may represent such a scenario and, in particular, indicate that the average inclination angle cannot predict its dynamic behavior. This emphasizes the importance in performing dynamic loading tests, as described in this work, which can characterize the actual kinetic response of a given twin boundary.

VI. SUMMARY

A simple experimental setup is presented that allows both macroscopic and microscopic characterization of the dynamic response of an MSM crystal. Dynamic uniaxial loading using a commercial solenoid leads to twinning reorientation in the tested sample, which is monitored via force and displacement measurements. The collected data reveal the overall kinetics of the sample, i.e., the basic relation between the sample's deformation rate and the force that acts on it. This relation is vital for characterizing the quality of the crystal and for simulating its dynamic response as a magnetomechanical actuator. In particular, the experimental conditions are tuned such that the velocity of the sample spans the relevant range for actuation and allows detecting the transition force from the slow thermally activated response to a-thermal fast response. Complementary high speed imaging allowed microscopic evaluation of the motion of individual twin boundaries within the sample and for the correlation of this twin boundary motion with the macroscopic response of the crystal.

ACKNOWLEDGMENTS

This research was supported by the United States-Israel Binational Science Foundation (BSF; Grant No. 2016662) and the National Science Foundation through Grant No. NSF-DMR-1710640.

REFERENCES

[1] K. Ullakko, J. K. Huang, C. Kantner, R. C. O'Handley, and V. V. Kokorin, Appl. Phys. Lett. **69**, 1966 (1996).
[2] P. Müllner, V. A. Chernenko, and G. Kostorz, J. Appl. Phys. **95**, 1531 (2004).
[3] M. Kohl, M. Gueltig, V. Pinneker, R. Yin, F. Wendler, and B. Krevet, Micromachines **5**, 1135 (2014).
[4] M. Chmielus, X. X. Zhang, C. Witherspoon, D. C. Dunand, and P. Mullner, Nat. Mater. **8**, 863 (2009).
[5] E. Faran and D. Shilo, Exp. Tech. **40**, 1005 (2016).
[6] E. Faran and D. Shilo, Appl. Phys. Lett. **100**, 151901 (2012).
[7] E. Faran and D. Shilo, Smart Mater. Struct. **25**, 095020 (2016).
[8] V. A. Chernenko, V. A. L'vov, P. Müllner, G. Kostorz, and T. Takagi, Phys. Rev. B **69**, 134410 (2004).
[9] I. Aaltio, O. Söderberg, Y. Ge, and S.-P. Hannula, Scr. Mater. **62**, 9 (2009).
[10] L. Straka, N. Lanska, K. Ullakko, and A. Sozinov, Appl. Phys. Lett. **96**, 131903 (2010).
[11] R. I. Barabash, C. Kirchlechner, O. Robach, O. Ulrich, J.-S. Micha, A. Sozinov, and O. M. Barabash, Appl. Phys. Lett. **103**, 021909 (2013).
[12] L. Straka, O. Heczko, H. Seiner, N. Lanska, J. Drahokoupil, A. Soroka, S. Fähler, H. Hänninen, and A. Sozinov, Acta Mater. **59**, 7450 (2011).
[13] A. Sozinov, N. Lanska, A. Soroka, and L. Straka, Appl. Phys. Lett. **99**, 124103 (2011).
[14] D. Kellis, A. Smith, K. Ullakko, and P. Müllner, J. Cryst. Growth **359**, 64 (2012).
[15] O. Heczko, J. Kopeček, L. Straka, and H. Seiner, Mater. Res. Bull. **48**, 5105 (2013).
[16] E. Faran and D. Shilo, Mater. Sci. Technol. **30**, 1545 (2014).
[17] Y. Ge, O. Heczko, O. Söderberg, and S.-P. Hannula, Scr. Mater. **54**, 2155 (2006).
[18] A. Pramanick, X.-L. Wang, A. D. Stoica, C. Yu, Y. Ren, S. Tang, and Z. Gai, Phys. Rev. Lett. **112**, 217205 (2014).
[19] E. Faran and D. Shilo, J. Mech. Phys. Solids **59**, 975 (2011).
[20] E. Faran and D. Shilo, J. Mech. Phys. Solids **61**, 726 (2013).
[21] E. Faran, L. Riccardi, and D. Shilo, Shape Mem. Superelasticity **3**, 206 (2017).
[22] A. Saren, D. Musiienko, A. R. Smith, and K. Ullakko, Scr. Mater. **113**, 154 (2016).
[23] A. Saren, T. Nicholls, J. Tellinen, and K. Ullakko, Scr. Mater. **123**, 9 (2016).
[24] N. Zreihan, E. Faran, and D. Shilo, Scr. Mater. **144**, 44 (2018).
[25] Z. Li, Y. Zhang, C. Esling, X. Zhao, and L. Zuo, Acta Mater. **59**, 3390 (2011).
[26] L. Straka, O. Heczko, and H. Hänninen, Acta Mater. **56**, 5492 (2008).

[27]R. Chulist, E. Pagounis, A. Böhm, C. G. Oertel, and W. Skrotzki, Scr. Mater. **67**, 364 (2012).
[28]N. Zreihan, A. Krimer, D. Avisar, E. Pagounis, D. Shilo, and E. Faran, Funct. Mater. Lett. **12**, 1850102 (2019).
[29]E. Faran, I. Benichou, S. Givli, and D. Shilo, J. Appl. Phys. **118**, 244104 (2015).
[30]N. Zreihan, E. Faran, and D. Shilo, Appl. Phys. Lett. **107**, 041605 (2015).
[31]R. Chulist, L. Straka, N. Lanska, A. Soroka, A. Sozinov, and W. Skrotzki, Acta Mater. **61**, 1913 (2013).
[32]O. Heczko, L. Straka, and H. Seiner, Acta Mater. **61**, 622 (2013).
[33]H. Seiner, R. Chulist, W. Maziarz, A. Sozinov, O. Heczko, and L. Straka, Scr. Mater. **162**, 497 (2019).
[34]L. Straka, A. Soroka, H. Seiner, H. Hänninen, and A. Sozinov, Scr. Mater. **67**, 25 (2012).